Hindawi
Geofluids
Volume 2023, Article ID 9444486, 15 pages
https://doi.org/10.1155/2023/9444486

Research Article

Application and Principle of Bolt-Mesh-Cable Control Technology in Extremely Soft Coal Seam Roadway

Fengfeng Wu[1,2] **Jian Zhang**[1,2] **Ping Wang**[3] **Xiaofeng Zhao**[3] **Yanwei Xuan**[3] **Bo Lv**[1,2] **Jinkai Wei**[1,2] **Zhiqiang Gao**[1,2] **Shibao Liu**[1,2] **and Haoyuan Gu**[1,2]

[1]*Key Laboratory of Deep Coal Resource Mining, Ministry of Education, China University of Mining and Technology, Xuzhou 221116, China*
[2]*School of Mines, China University of Mining and Technology, Xuzhou 221116, China*
[3]*Henan Shenhuo Xinglong Mining Co., Ltd., Xuchang 461000, China*

Correspondence should be addressed to Fengfeng Wu; wufengfeng@cumt.edu.cn

Received 28 October 2022; Revised 24 November 2022; Accepted 27 March 2023; Published 4 May 2023

Academic Editor: Jinpeng Zhang

The extremely soft coal seam roadway has the problems of low surrounding rock strength and difficult support. Based on the engineering background of the mining roadway in the extremely soft coal seam of the Quandian coal mine, this paper adopts the research method combining numerical simulation and field measurement. The stress field, displacement field, support force, and loading arch structure characteristics of roadway surrounding rock under bolt-mesh-cable support and existing shed-cable support are compared, and the control principle of bolt-mesh-cable in extremely soft coal seam roadway is expounded. Our study indicated that compared with nonsupport and shed-cable support, the pressure stress range of the surrounding rock in extremely soft coal seam increases, and the stress gradient decreases when bolt-mesh-cable support is used. The roadway displacement and displacement difference decrease. The components of the support achieve stress coordination. The thickness of the loading arch formed in the surrounding rock is large, and the compressive stress in the arch is evenly distributed. The bolt-mesh-cable significantly improves the stress environment and the stability of the roadway. The field practice shows that the roadway deformation is small after the bolt-mesh-cable support is adopted, and the roadway section during excavation and mining meets the requirements of safety production.

1. Introduction

As a kind of active support method with high strength and low cost, bolt-mesh-cable support (BMC-S) has gradually become the mainstream of mining roadway support in Chinese coal mines because it can significantly improve the stability of surrounding rock. In recent years, with the increasing intensity of coal mining, the proportion of extremely soft coal mining is also growing. However, it is generally believed that BMC-S is difficult to control the deformation of the roadway and surrounding rock in extremely soft coal seam [1–3] and cannot guarantee the deformation of support and surrounding rock and the coupling coordination between the supporting components [4]. Therefore, most of the roadway support still adopts shed or shed-cable support. In order to promote the application of BMC-S in extremely soft coal roadways, the control principle of BMC-S in extremely soft coal roadways needs to be further studied.

Domestic and foreign scholars have conducted a lot of research and exploration on the support theory and control technology of soft coal roadway surrounding rock [5–8]. He et al. [9] believed that the failure of soft rock roadway was mainly caused by the uncoupling of mechanical properties of support and surrounding rock and proposed the bolt-mesh-cable coupling support technology to strengthen the support of key parts of roadway surrounding rock, which realized the coordinated deformation of support and surrounding rock. Wang et al. [10] studied the stress of different parts of the roadway in three soft coal seams with large dip angles, pointed out that the roof of the roadway and the upper and middle parts of the high rib were prone to deformation and failure,

and put forward the support concept of "strong rib fixing and strong roof protection"; Jing et al. [11, 12] studied the formation mechanism of anchorage structure in tectonic soft coal and calculated the bolt preload required to form stable anchorage structure in tectonic coal. Yu et al. [13] put forward the concept of "weak structure" and the control technology of high-strength prestressed anchor basic support, weak structure strengthening support for asymmetric deformation, and long-term rheological characteristics of soft rock roadway. By means of numerical calculation, Yu et al. [14, 15] analyzed that the support failure of weak semicoal rock roadway can be divided into several stages, such as joint fissure development, rock fragmentation deformation, stress superposition, and rheological and large deformation, and put forward the supporting technology of "truss + bolt-mesh-cable." Dan et al. [16] thought that the side and corner are the key parts of the soft broken surrounding rock roadway support. Strengthening the support strength of the side and corner can enhance the overall stability of the roadway and put forward the strong side and strong angle bolt support control technology. Yun et al. [17] aimed at the soft roof soft coal mining roadway after multiple repairs, believed that the stability of surrounding rock can be improved by improving the bearing capacity of surrounding rock, and put forward the combined support scheme of advanced pipe shed + grouting and permanent bolt-cable + shotcrete; Lu et al. [18] simulated and studied the surrounding rock activity law of soft coal roadway in the thick coal seam, believed that the two sides were always the focus of support control, and proposed the surrounding rock control principle of strengthening the bottom side angle and the two sides support. Huang et al. [19] pointed out that the deformation and failure forms of inclined soft coal roadway are mainly tensile failure and shear failure and put forward the support design method of optimizing roadway section and anchor mesh support.

The above research results have achieved good results in soft coal roadway support engineering but more focus on general soft coal roadway surrounding rock control theory and technology. There are relatively few studies on the control principle of BMC-S in extremely soft coal seam roadways with compressive strength of less than 5 MPa [20, 21]. Based on the engineering background of 11000 working face transportation roadways in the Quandian coal mine, this paper uses UDEC software to study the stress field, displacement field distribution characteristics, support stress characteristics, and loading arch structure characteristics of extremely soft coal seam roadway. The research reveals the control principle of BMC-S in extremely soft coal seam roadway, in order to provide a reference for the design of coal roadway support under similar conditions.

2. Engineering Background

2.1. Occurrence Characteristics of Surrounding Rock. Quandian coal mine is located between Yuzhou city and Xuchang county in the eastern part of the Yuzhou mining area. The 11000 working faces are located in the northeast of 11 mining areas in the east wing of the minefield. The main coal seam is no. 2-1 coal seam with a depth of about 400 m. The thickness of the coal seam is 2.8 ~ 12.5 m, with an average of 4.59 m. The dip angle is 27°, and the Pu coefficient is only 0.15~0.2. There is no mining influence around. The direct top of the coal seam is mainly sandy mudstone and siltstone with a thickness of 1.5 ~ 5 m. The direct bottom is mainly sandy mudstone and siltstone with a thickness of 2.5 ~ 5 m. The geological comprehensive histogram of the working face is shown in Figure 1. The in situ stress test results show that the underground stress field is dominated by tectonic stress, and the maximum principal stress is in the horizontal direction, which is 15.7 MPa.

2.2. Support Method and Deformation Characteristics of Roadway. The transportation roadway of 11000 working faces is excavated along the coal seam floor. The section is a straight wall semicircular arch, with a net width of 5200 mm, a net height of 4000 mm, and a wall height of 1400 mm. The original support adopts "shed-cable" combined support. The 36 U type shed is 5355 mm × 3700 mm, the shed distance is 700 mm, the cable is Φ18.9 mm, L8000 mm prestressed steel strand, and the spacing is 2000 mm × 1400 mm. The roadway support parameters are shown in Figure 2(a).

Before the installation of equipment in 11000 working faces, the deformation of the roadway was very serious, and the floor heave and roof subsidence were serious. The floor heave is greater than the roof subsidence, and the floor heave reaches 600-800 mm locally, resulting in track deviation. The approaching amount of the high side is greater than that of the low side, and the maximum approaching the amount of the two sides is up to 925 mm. The 36 U shed arch beam is seriously deformed or even broken, and the maximum deformation reaches 500 mm. The deformation of the roadway and the failure characteristics of support are shown in Figure 2(b).

3. Modelling

The discrete element software UDEC2D7.0 was used to establish the plane strain model [22–24]. The size of the model was 50 m × 50 m. The bottom boundary of the model was a fixed boundary, the left and right boundaries were displacement boundaries, and the top boundary was the stress boundary. The top of the model was subjected to 10 MPa vertical stress (equivalent to the self-weight stress of the overlying 400 m rock layer). The lateral pressure coefficient was set to 1.5 according to the ground stress test results. The roadway was located in the middle of the model and was excavated along the roof of no. 2-1 coal seam. Since the two sides of the roadway are extremely soft coal and the mechanical strength is very low, the key to ensure the stability of the roadway is the control effect of the two sides [25]. Therefore, the research focus is set to the two sides. In the model, two monitoring lines with a length of 20 m are set along the middle of the two sides parallel to the coal seam dip direction, and 10 measuring points are evenly arranged in each line. The numerical calculation model and the layout of the measuring lines are shown in Figure 3.

Rock formation	Histogram	Height/m	Lithology
Fine-sandstone		7.45	Dark gray, fracture development
Sandy mudstone		4	Gray, fissured, broken core
No. 2-1 coal seam		4.7	Black, powdery, granular, soft and broken
Mudstone		3.4	Gray black, soft and fragile
Sandy mudstone		10.7	Dark gray, thick layered, dense and complete

Figure 1: Comprehensive geological bar chart of working face.

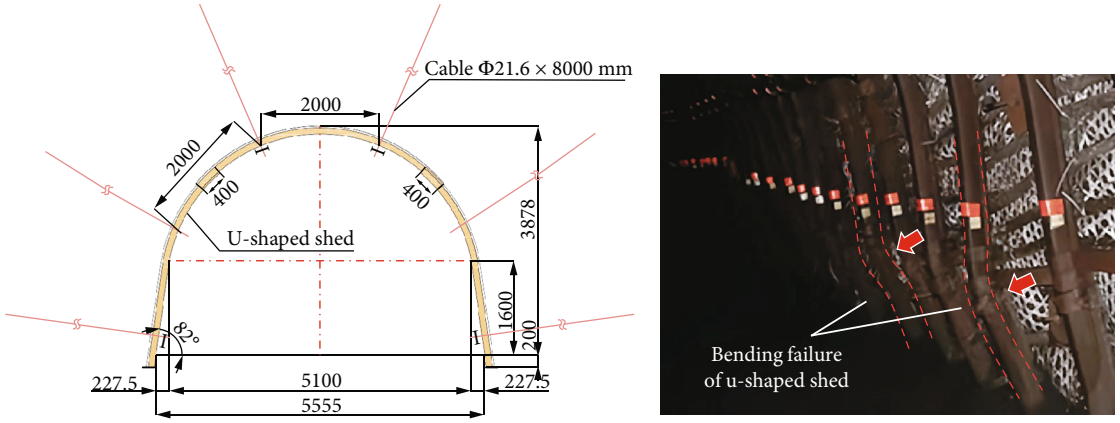

(a) Support method

(b) Scene shed leg kneeling down

Figure 2: Existing support methods and deformation characteristics.

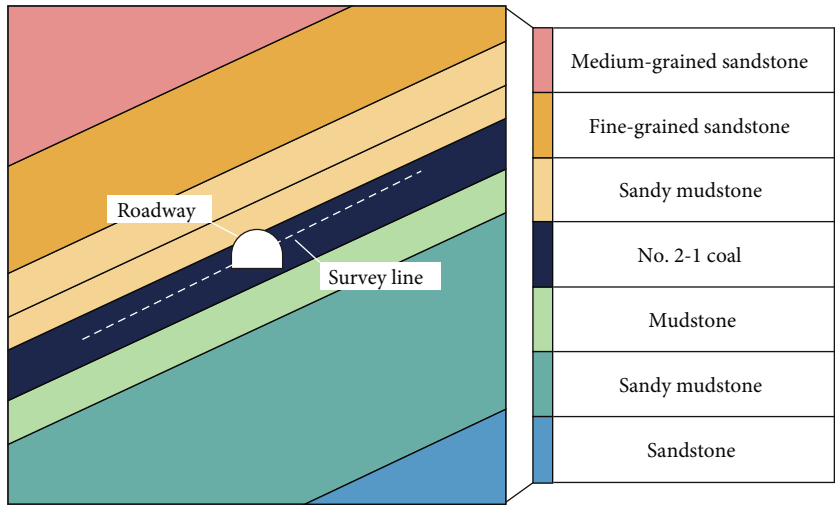

Figure 3: Numerical calculation model.

The Mohr-Coulomb yield criterion is used in the calculation process. The physical and mechanical parameters of coal and rock mass and joints in the model are shown in Tables 1 and 2, respectively. The parameters of coal and rock mass are obtained on the basis of rock mechanical parameters obtained by laboratory mechanical tests and reduced by the GSI rock mass classification method [26, 27].

The stress and deformation of the surrounding rock under three support modes—no support, shed-cable support—and BMC-S, are numerically simulated. Based on the

Table 1: Physical and mechanical parameters of coal and rock mass in the model.

Lithologic characters	Density(kg·m^{-3})	Volume modulus (GPa)	Shear modulus (GPa)	Angle of internal friction (°)	Cohesion (MPa)	Tensile strength (MPa)
Medium-grained sandstone	2500	10.2	7.0	30	6.6	1.9
Fine-grained sandstone	2600	39.3	28.3	35	11.4	5.8
Sandy mudstone	2530	1.3	0.7	29	5.5	2.8
No. 2-1 coal	1420	2.1	0.5	20	0.8	0.15
Mudstone	2520	2.7	1.6	28	5.1	2.6
Sandy mudstone	2580	45.3	31.2	33	9.7	5.2
Sandstone	2510	2.5	1.6	27	4.5	2.5

Table 2: Mechanical parameters of the structural plane in the model.

Structural plane	Normal stiffness (GN·m^{-1})	Tangential stiffness (GN·m^{-1})	Angle of internal friction (°)	Cohesion (MPa)	Tensile strength (kPa)
Medium-grained sandstone	362	145	18	1.5	1.2
Fine-grained sandstone	164	66	15	1.0	1.0
Sandy mudstone	126	50.3	12	0.5	1.0
No. 2-1 coal	12	4.8	10	0.4	0.6
Mudstone	89.8	35.9	12	0.4	0.8
Sandy mudstone	167	66.8	15	0.1	1.0
Sandstone	166	66	20	1.5	1.2

Table 3: Mechanical parameters of U-shaped shed.

Support material	Model	Cross sectional area/cm^2	Theoretical weight/kg/m	Allowable stress/MPa	Allowable bending moment/kN·m
U-shaped shed	36 U	45.7	35.8	520	40

Table 4: Mechanical parameters of bolt-mesh-cable.

Support material	Diameter/mm	Dimension/mm	Yield strength/MPa	Rupturing load/kN	Pretightening force/kN
Bolt	22	2600	335	167	60
Cable	21.6	8000/4000	—	607	180
Mesh	4	3600 × 900	235	6	—

concept of BMC-S with high preload and high stiffness, the physical and mechanical parameters of support materials used in the model are shown in Tables 3 and 4.

4. Interaction Characteristics of the Surrounding Rock and Support

4.1. Characteristics of Stress Field of the Surrounding Rock. According to the Mohr-Coulomb strength criterion, when the strength of the surrounding rock is constant, the failure of the surrounding rock mainly depends on the maximum principal stress and shear stress of the surrounding rock [28–30]. Therefore, this section focuses on the analysis of the influence law of different supports on the maximum principal stress field and shear stress field of the surrounding rock in an extremely soft coal roadway, so as to explain the mechanism of BMC-S.

4.1.1. Maximum Principal Stress Field. Figure 4 is the maximum main stress field distribution nephogram of the roadway surrounding rock under different supporting methods.

In Figure 4, it can be seen that the main stress field of the surrounding rock is spread to the surrounding and shows nonuniformity. According to the stress state of the surrounding rock, it can be divided into a tensile stress zone and a compressive stress zone. Under different supporting methods, the distribution range of the tensile stress zone of the surrounding rock is significantly different, as shown in Table 5.

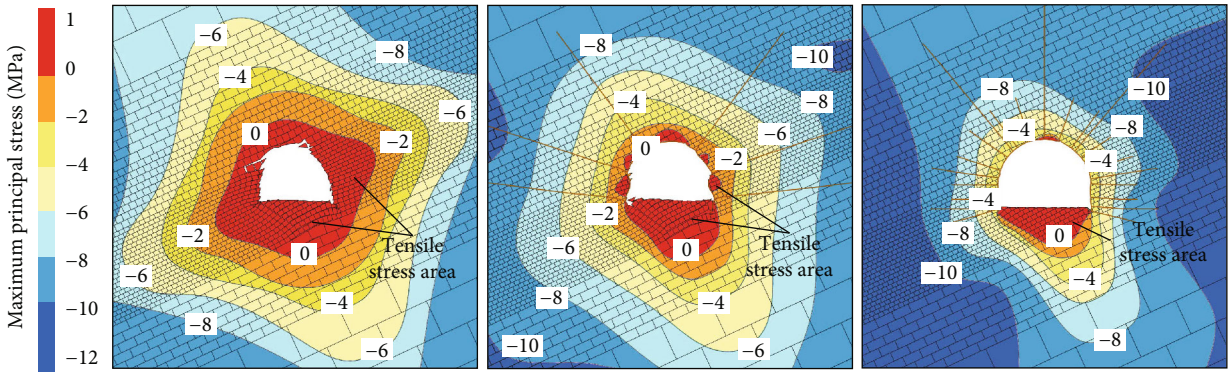

(a) Non-support (b) Shed-cable (c) Bolt-mesh-cable

Figure 4: Distribution nephogram of maximum principal stress of the surrounding rock under different supports.

Table 5: Distribution characteristics of tensile stress zone of the surrounding rock under different supports.

Supporting method	Tensile stress zone/m			Maximum tension stress	
	Roof	Floor	Ribs	Value/MPa	Position
Nonsupport	2	4	3	0.8	Floor
Shed-cable	0.6	4	0.8	1	Floor
Bolt-mesh-cable	0	2	0	0.6	Floor

Table 5 shows that the tensile stress area of the surrounding rock is 2 ~ 4 m without support. After using shed-cable support, the tensile stress area of the roof and two sides is reduced to 0.8 m, but the tensile stress area of the floor changes little. After the BMC-S is adopted, the tensile stress area of the roof and two sides is reduced to a very small range, nearly 0, and the tensile stress area of the floor is also reduced to 2 m, which is 50% less than that without the support and shed-cable support. In addition, the maximum tensile stress of the surrounding rock with different support from large to small is shed-cable support, no support, and BMC-S. The maximum tensile stress of the surrounding rock under shed-cable support is 1 MPa. The maximum tensile stresses of the surrounding rock without the support and BMC-S are 0.8 MPa and 0.6 MPa, respectively, which are 20% and 40% less than that of shed-cable support. They are all located in the basic bottom strata 1.5 m away from the bottom edge. This shows that under the condition that no supporting measures are taken on the floor of the roadway, the BMC-S can still effectively eliminate the tensile stress in the floor surrounding rock, and the shed-cable support will aggravate the tensile failure of the floor surrounding rock.

In order to further quantify the stress distribution characteristics of the surrounding rock under different supporting methods, the concept of stress gradient (Formula (1)) is introduced. A larger stress gradient will lead to tensile or shear failure of coal and rock mass [31].

$$T_\sigma = \left|\frac{\partial \sigma}{\partial s}\right|. \quad (1)$$

In the formula, T_σ is stress gradient, MPa/m, σ is stress variation in unit length, MPa, s is unit length, m.

The maximum principal stress of the surrounding rock is extracted from the survey line of two sides of the roadway, and the stress gradient T_σ is calculated according to Formula (1). Due to the coal seam having a certain dip angle, the high side is more prone to structural instability than the low side. Here, only the high side is selected for analysis. The results are shown in Figure 5.

In Figure 5(a), it can be seen that although the stress of the surrounding rock on the high side of the roadway increases gradually with the increase of depth until it recovers to the original rock stress; at the same depth, the stress level of the surrounding rock supported by BMC-S is the highest, and the stress level of the surrounding rock without support is the lowest. In Figure 5(b), the stress gradient T_σ of the surrounding rock without support is less than 1 MPa/m in the shallow part, which increases rapidly to the peak value and then decreases gradually with the increase of the depth of the surrounding rock. The characteristics of a small stress gradient in the shallow part of the surrounding rock are consistent with the serious fragmentation of the shallow surrounding rock in this way. After using shed cable and BMC-S, T_σ gradually decreases as a negative exponential function and, finally, tends to 0. The average value of T_σ surrounding rock under shed-cable support is 1.25 MPa/m and that under BMC-S is 0.98 MPa/m, which decreases by 21.6%. It can be seen that the BMC-S cannot only significantly improve the stress level of the surrounding rock but also effectively reduce the principal stress gradient inside the surrounding rock, so as to control the deformation of the surrounding rock.

4.1.2. Shear Stress Field. The distribution characteristics of the shear stress field of the surrounding rock under different supporting methods are shown in Figure 6.

It can be seen in Figure 6 that without support, the roof and floor of the roadway formed obvious shear stress concentration. With the increase of the surrounding rock depth, the shear stress increased first and then decreased. The maximum peak point was located in the basic bottom rock at 8 m from the edge of the floor, reaching 9 MPa. The changing trend of shear stress on the two sides is generally consistent with the roof and floor,

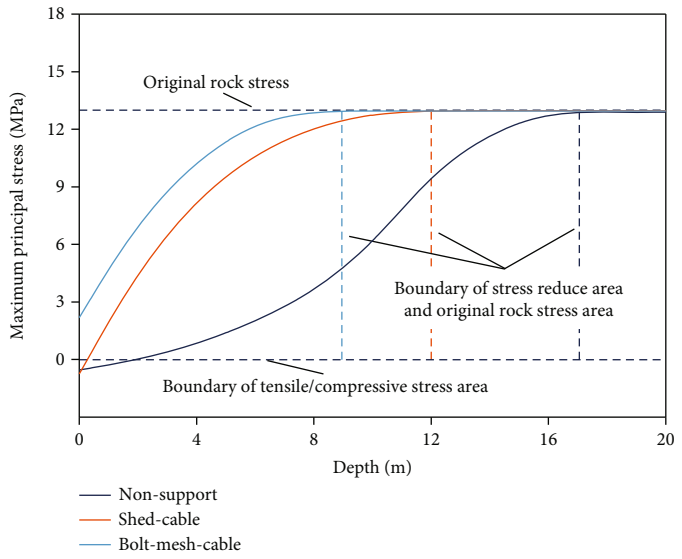

(a) Stress variation curve

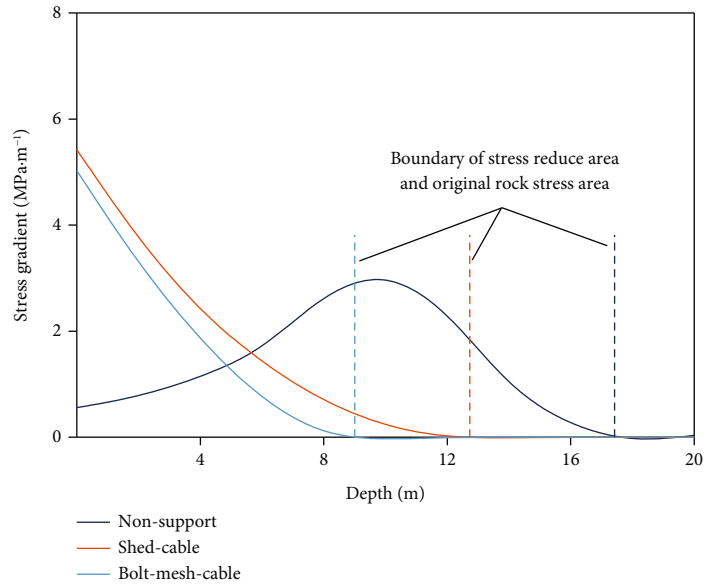

(b) Stress gradient

Figure 5: Variation characteristics of the maximum principal stress of the roadway surrounding rock with different supports.

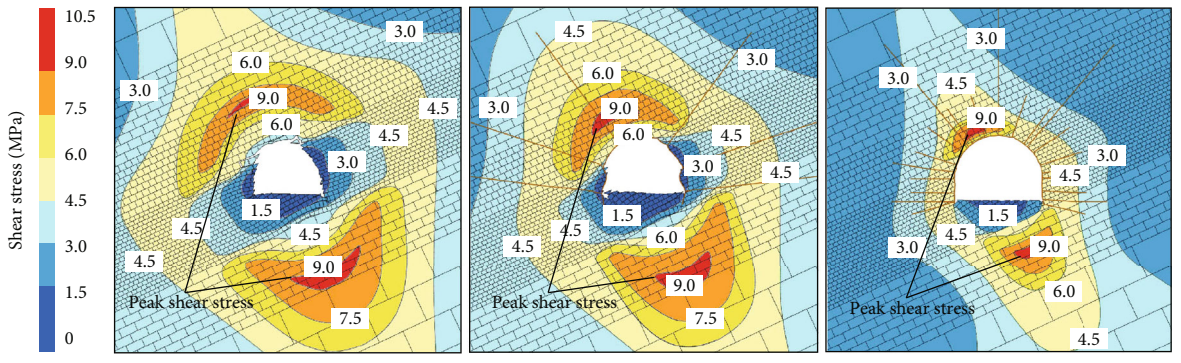

(a) Non-support (b) Shed-cable (c) Bolt-mesh-cable

Figure 6: Distribution nephogram of shear stress of the surrounding rock under different supports.

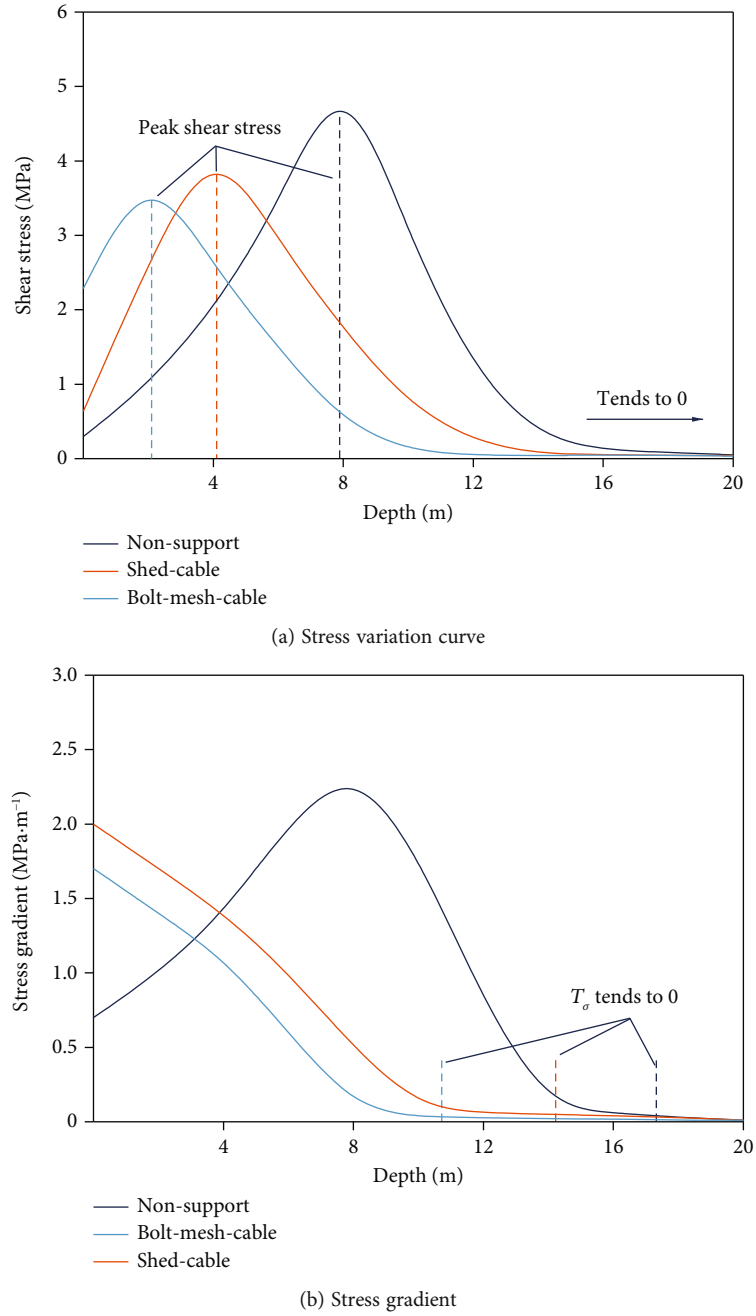

(a) Stress variation curve

(b) Stress gradient

Figure 7: Variation characteristics of shear stress in the surrounding rock with different supports.

and the maximum peak point is located 7 m away from the surface of the coal body on the high side, which is only 5.3 MPa. This is mainly because the strength of the extremely soft coal body on the side is low and the bearing capacity is poor. When the stress concentration exceeds the strength of the coal body, the shear failure of the coal body will occur, leading to the peak shear stress further migrating to the deep surrounding rock or the upper hard rock [32]. Under shed-cable support, the peak shear stress of the roof and two sides shifts to the shallow surrounding rock, and the depths are reduced to 2 m and 4 m, respectively, which are 33% and 43% lower than those without support, but the position of floor peak point does not change significantly, and the peak value reaches 10.4 MPa, which is 1.4 MPa higher than that without support. After the BMC-S was adopted, the peak shear stress of the roof and the two sides shifted to the shallow surrounding rock again. The distance from the roof to the roadway surface was less than 1 m, which was an average decrease of 64% compared with that of the shed-cable support. The peak shear stress of the floor also began to shift to the roadway surface, which was 3 m away from the edge of the floor and 63% less than that of the shed-cable support. The peak shear stress was reduced to 9.2 MPa, and the concentration of shear stress was significantly reduced.

The distribution law of shear stress in high-side coal of roadway is shown in Figure 7.

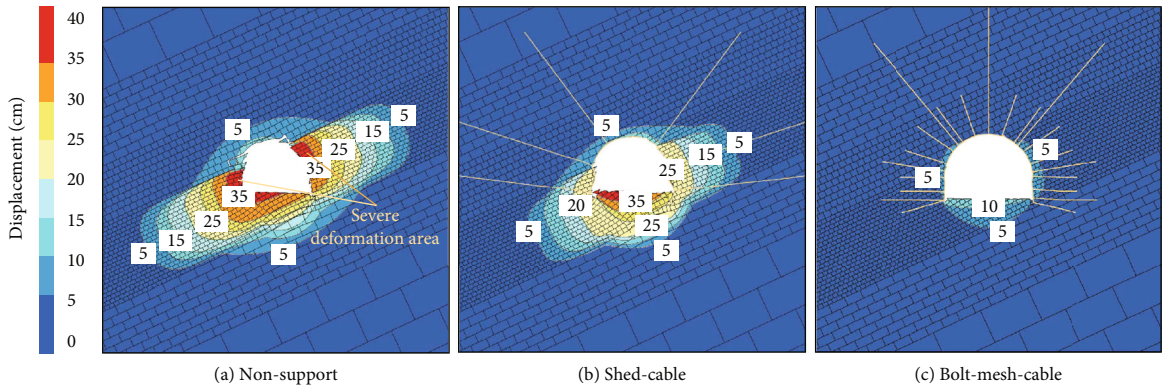

Figure 8: Distribution nephogram of displacement of the surrounding rock with different supports.

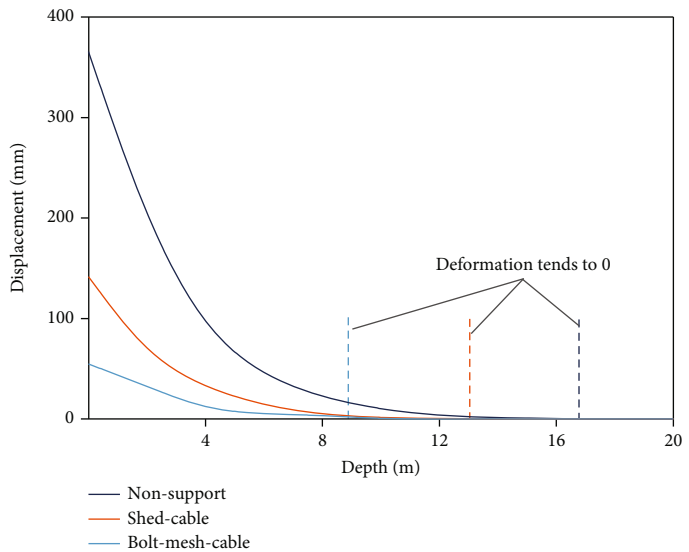

(a) Displacement curve

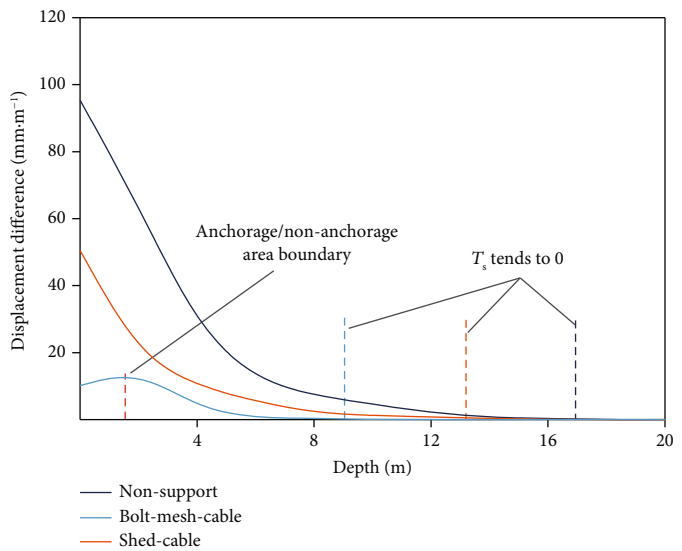

(b) Displacement difference curve

Figure 9: Displacement characteristics of the surrounding rock with different supports.

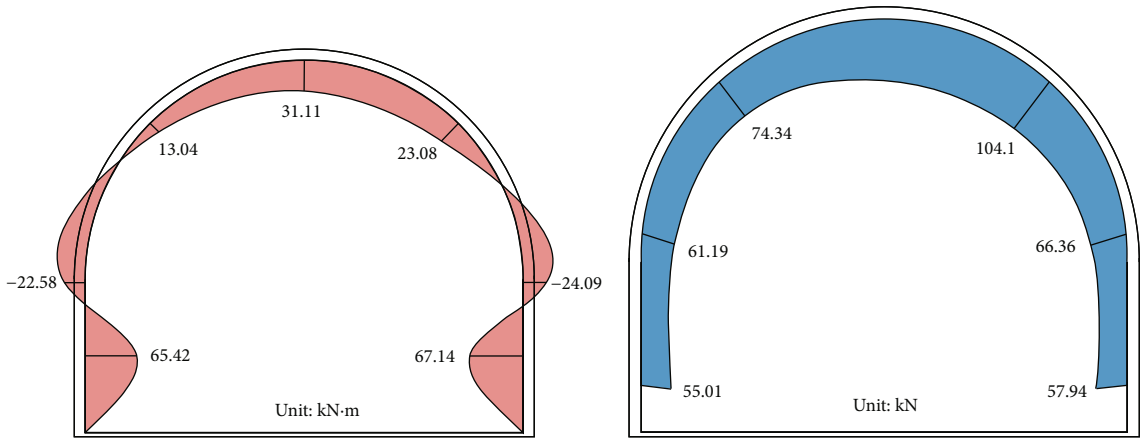

(a) U-shaped shed-bending moment distribution (b) Axial force distribution of cable

Figure 10: Mechanical characteristics of shed-cable support.

It can be seen that the various characteristics of high-side stress are similar to the distribution characteristics of a nephogram, that is, the moving distance of the peak shear stress of coal body to the roadway surface under the BMC-S is significantly greater than that under the shed-cable support, as shown in Figure 7(a). It can be seen in Figure 7(b) that the average stress gradient T_σ of the surrounding rock with shed-cable support is 0.73 MPa/m and that with BMC-S is 0.52 MPa/m, which is reduced by 28.8%, indicating that BMC-S can effectively reduce the shear stress gradient in the surrounding rock and reduce the possibility of shear failure of the surrounding rock.

4.2. Displacement Field Characteristics of Surrounding Rock. Affected by the large dip angle of the coal seam, the displacement of the roadway often presents the characteristics of asymmetry around, which is reflected in the serious deformation of the surrounding rock in the middle and upper part of the high side and the middle and lower part of the low side, as shown in Figure 8.

It can be seen in Figure 8 that under the conditions of no support and shed-cable support, the roof and floor convergence of the roadway is 471 mm and 392 mm, respectively, and the two sides' convergence is 854 mm and 506 mm, respectively. The overall deformation of the surrounding rock is serious. The maximum displacement of the roof and floor and two sides is only 137 mm and 112 mm, which is 65% and 78% lower than that of shed-cable support, respectively. The severe deformation of the surrounding rock is effectively inhibited.

When the coal-rock mass is deformed under force, the displacement difference will be formed due to the different displacement values at various positions inside the coal-rock mass. Displacement difference is composed of elastic-plastic deformation and structural plane (bedding, joints, cracks, etc.) deformation of coal and rock mass [33, 34], which can reflect the internal damage of coal and rock mass.

$$T_S = \left|\frac{\partial S}{\partial s}\right|. \quad (2)$$

In the formula, T_S is the displacement difference, mm/m, S is the displacement variation in unit length, mm, s is the unit length, m. Here, the displacement difference T_S is used as an index to measure the internal damage degree of surrounding rock, and the displacement variation law of coal body in the roadway high side is shown in Figure 9.

It can be seen from Figure 9 that no matter what kind of support method, the displacement of the high-side coal body decreases with the increase of the surrounding rock depth. When there is no support, the surface displacement of the high-side coal body reaches 336 mm, and the maximum internal displacement difference $T_{S\ \max}$ reaches 95.4 mm/m, indicating that the surrounding rock is seriously damaged, and there is obvious separation. In the shed-cable support, the displacement of the coal surface is 142 mm, and the maximum displacement difference $T_{S\ \max}$ in the surrounding rock is 50.5 mm/m, which is 61% and 47% less than that without support, respectively. The surface displacement of the coal body is only 54.8 mm, which is reduced by 63% compared with the shed-cable support. The maximum displacement difference $T_{S\ \max}$ of the surrounding rock is only 14.8 mm/m, which occurs at the end of the anchor end, which is reduced by 72%. It can be seen that the BMC-S can effectively inhibit the interlayer dislocation and sliding of the joint surface in the surrounding rock, reduce the damage of the surrounding rock, and maintain the continuity and stability of the coal body.

4.3. Stress Characteristics of Support. The key to give full play to the supporting performance is to realize the coupling and coordination of the force between the supporting components [35, 36]. Under the support of the shed and cable, the stress characteristics of 36 U shed and cable are shown in Figure 10.

It can be seen in Figure 10 that the bending moment of the two sides of the U-shaped shed is generally higher than that of the arch, and the maximum bending moment occurs on the high side, which is 67.14 kN m, exceeding the allowable bending moment of the shed, resulting in the displacement of the shed leg to the inside, and serious distortion

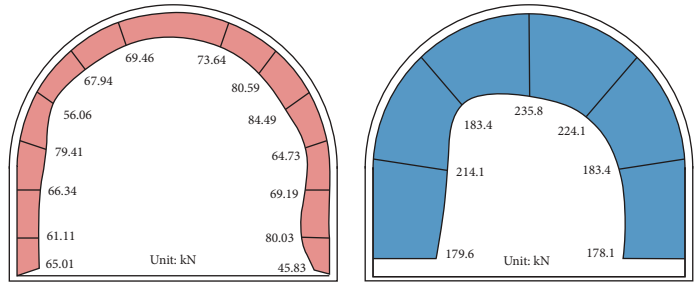

(a) Bolt axial force distribution

(b) Cable axial force distribution

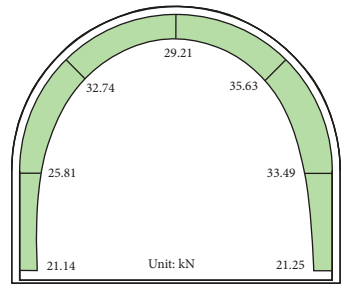

(c) Ladder axial force distribution

Figure 11: Stress characteristics of BMC-S.

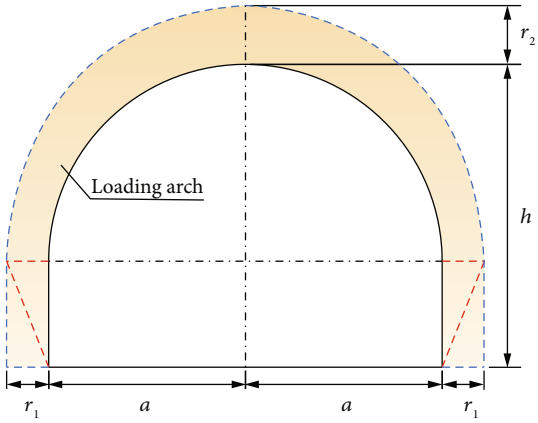

Figure 12: Loading arch schematic.

deformation, which is consistent with the abovementioned deformation characteristics. For the cable, the axial force is generally low, and the maximum axial force is 104.1 kN, which occurs at the high-side shoulder socket. The average axial force is 69.5 kN, only reaching 11.2% of the breaking load of the cable, and the load utilization rate is low. The main reason is that in the shed-cable support, due to the small shrinkage of the shed body and the poor effect of the cooperative support with the cable, the initial support resistance of the shed-cable support is small, and there is still a certain gap between the shed body and the surrounding rock, which cannot timely control the instantaneous and strong deformation of the ultrasoft coal body in the shallow part of the roof after the roadway is excavated. However, the deep ultrasoft coal body is prone to shear failure. When the failure range is further extended to the anchorage section of the cable, the local coal body around the cable is broken, resulting in the failure of the anchor space, and the support performance of the cable cannot be fully developed.

Under the support of BMC-S, the stress characteristics of the bolt, cable, and ladder beam are shown in Figure 11.

It can be seen in Figure 11 that the stress of the bolt at the high shoulder socket is the largest, reaching 84.4 kN, and the average axial force of the bolt is 70.9 kN, reaching 55.8% of the yield load. The stress of the cable at the top is the largest, reaching 235.8 kN, and the average axial force reaches 196.2 kN, reaching 32.9% of the breaking load. The stress state of the cable is good. In Figure 11(c), the maximum axial force of the ladder beam occurs in the middle and upper part of the high side. The maximum axial force is 35.6 kN, and the average axial force is 29.3 kN, which is less than the allowable load of 52 kN. It can be seen that under the condition that the surrounding rock is an extremely soft coal seam, the high pretightening force cable and high stiffness protective surface components can coordinate with each other, so that the cable support structure can be in a good stress state, which ensures the role of cable support in the control of the surrounding rock [37].

4.4. Characteristics of Loading Arch. The goal of support is to form a stable loading arch in the surrounding rock of the roadway in the extremely soft coal seam. The greater the thickness of the loading arch and the higher the stress levels are, the stronger the stability of the surrounding rock is. According to Pu's theory, the mechanical model of the loading arch is established [38], as shown in Figure 12.

The maximum supporting radius should meet the following:

$$R_0 = \max\{r_1, r_2\}. \tag{3}$$

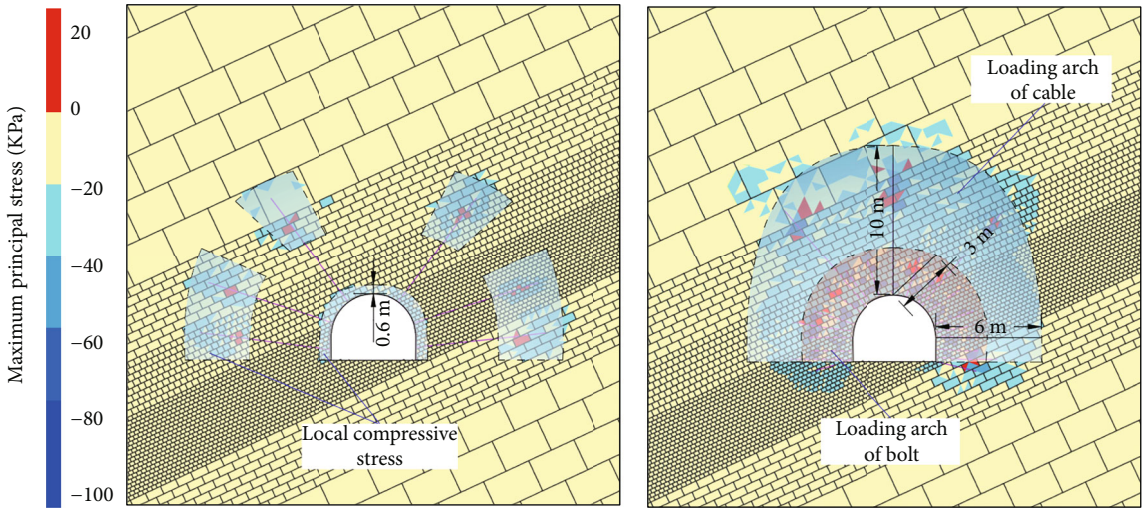

(a) Shed-cable

(b) Bolt-mesh-cable

Figure 13: Characteristics of the surrounding rock loading arch with different supports.

In the formula, R_0 is the maximum supporting radius, m; r_1 is the maximum support width, m; r_2 is the maximum support height, m; the values of r_1 and r_2 can be calculated as follows:

$$\begin{cases} r_1 = h \tan\left(45^\circ - \dfrac{\varphi}{2}\right) \\ r_2 = \dfrac{a + r_1}{f} \end{cases}. \tag{4}$$

In the formula, h is the height of the roadway, m, a is half of the span, m, φ is the internal friction angle of coal, and f is the hard coefficient of the roof.

The width of the 11000 transport roadways is 5.2 m, the height is 4 m, $\varphi = 20^\circ$, $f = 2$. Substituting Formulas (3) and (4), the maximum supporting radius of the surrounding rock is $R_0 = 2.7$ m. For the convenience of research, the stability index η is as follows:

$$\eta = \frac{R}{R_0}. \tag{5}$$

In the formula, R is the effective thickness of the loading arch; when $\eta \geq 1$, the surrounding rock is stable.

Since the support stress is much smaller than the original rock stress in magnitude, in order to analyze the loading arch structure characteristics formed by the support in the surrounding rock more accurately, the original rock stress is not considered in the simulation in this section. The simulation results are shown in Figure 13.

It can be seen in Figure 13 that when the shed cable is supported, the surrounding rock near the tail end of the cable and the front end of the anchorage section produces two compressive stress fields, and the end point of the cable is the center to diffuse around. The maximum compressive stress is 24.6 kPa, which appears in the roof anchorage section, and the maximum area radius is 4 m. With the distance from the anchorage section, the compressive stress value decreases gradually, and a large area of near-zero compressive stress area appears in the middle of the free section. This is because the shed-cable support cannot give full play to the active support performance of the cable, resulting in the isolated distribution of the compressive stress field formed in the anchorage section and the inability to connect with each other. Only a loading arch with a thickness of only 0.6 m is formed in the shallow surrounding rock near the shed side. The stability index of the surrounding rock is calculated to be $\eta = 0.2$, which is far less than 1, indicating that the shed-cable support cannot play an effective supporting role in the surrounding rock.

When the BMC-S is supported, the stress level of the compressive stress field formed by the bolt and cable increases, and the diffusion range increases. The compressive stress field formed by each anchor and cable is closely linked to the surrounding rock, forming a loading arch. The minimum supporting thickness of the loading arch reaches 6 m, and the surrounding rock stability index $\eta = 2.2$, greater than 1, which is 11 times of the shed-cable support. The maximum compressive stress in the arch reaches 86.25 kPa, and the average compressive stress reaches 46.5 kPa. The supporting effect is significantly improved. Among them, the loading arch formed by the bolt has a small thickness of 3 m, close to the surface of the surrounding rock, which can effectively increase the confining pressure of the shallow extremely soft coal body and improve the loading capacity of the coal body. The loading arch formed by cable has a large thickness of 6 ~ 10 m, which is closer to the deep or hard rock of the coal body. It can fully mobilize the loading capacity of the deep intact surrounding rock and improve the stability of an extremely soft coal body. The load-loading arch formed by bolts and cables overlaps with each other in the surrounding rock, forming a large active support area, which significantly inhibits the deformation and failure of the surrounding rock and the development of joint fissures in the loading arch, and can also withstand the deformation load of the rock mass outside the arch.

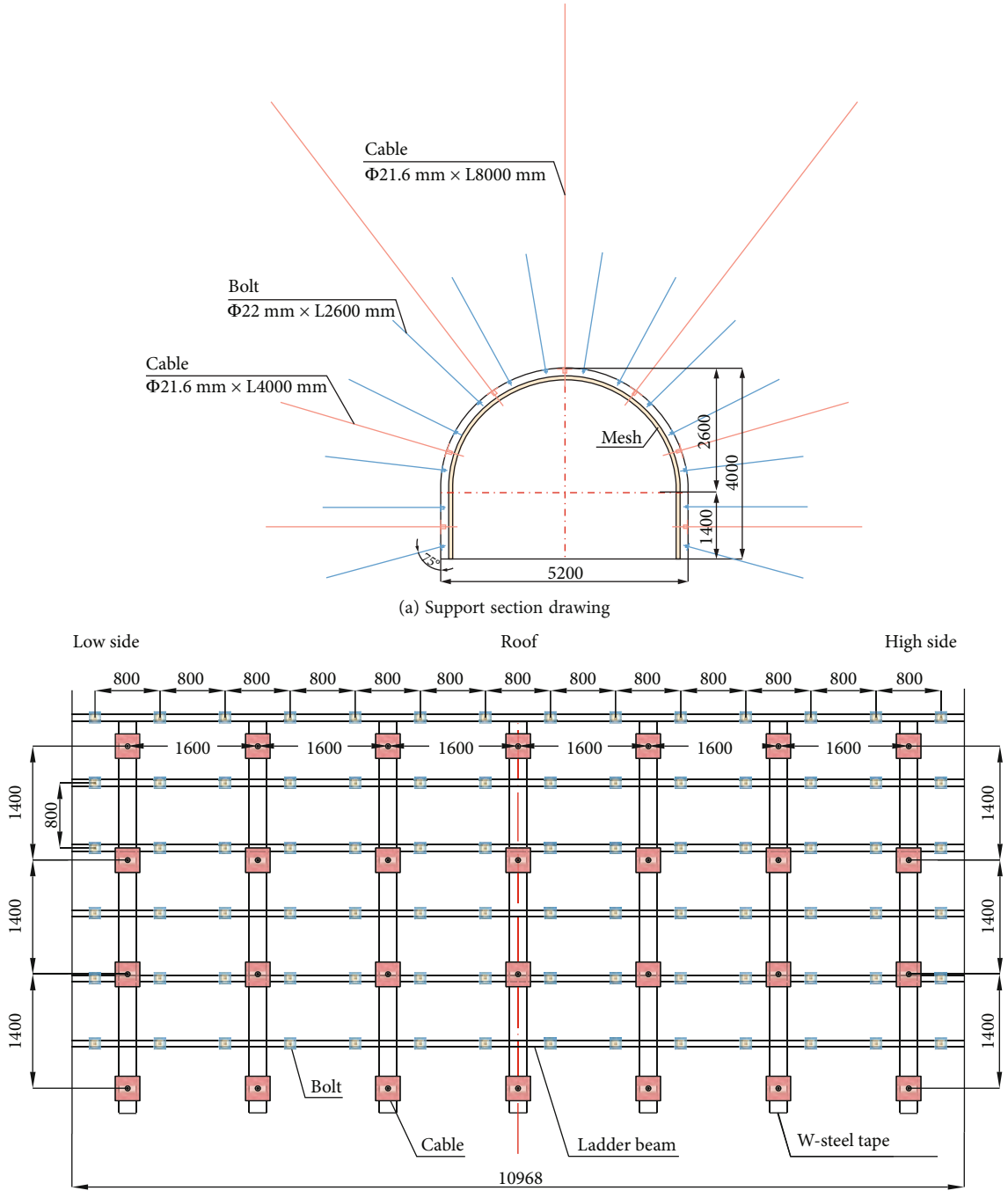

(a) Support section drawing

(b) Support deployment diagram

Figure 14: BMC-S scheme.

5. Engineering Practice

5.1. Bolt-Mesh-Cable Support Scheme. Combined with the above analysis, the support mode of 11000 working face transport crossheading is adjusted to BMC-S combined support. The bolt adopts Φ22 mm, L2600 mm left-handed non-longitudinal reinforcement spiral steel bolt, the spacing is 700 × 700 mm, and the preload torque is not less than 300 N m, with Φ12 mm steel ladder beam. The cable is Φ21.6 mm, L8000 mm (4000 mm), 1 × 19 steel strand, row spacing is 1400mm × 1400 mm, preload is not less than 200 kN, with BHW-280-3.0 W steel belt. Using plastic mesh + Q235 steel mesh guard, support scheme is shown in Figure 14.

5.2. Control Effect of the Surrounding Rock. During excavation and mining, the displacement station was arranged in the transport roadway of 11000 working faces, and the displacement change of roadway was monitored and counted

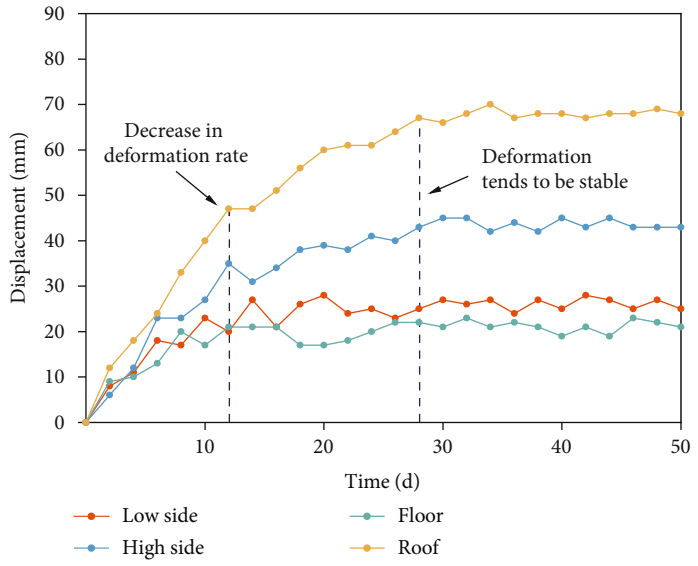

(a) During excavation

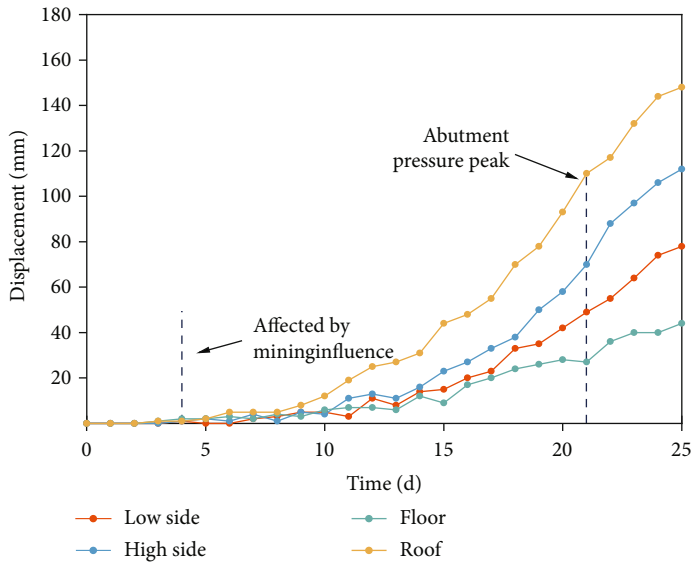

(b) During mining

Figure 15: Change curve of roadway displacement during excavation.

(a) During excavation (b) During mining

Figure 16: Field control effect of roadway surrounding rock.

by cross point method. The curve of roadway displacement change is shown in Figure 15.

It can be seen in Figure 15 that during the excavation, the maximum displacement of the roof and floor of the roadway is 89 mm, the maximum displacement of the two sides is 70 mm, and the mining period is 192 mm and 187 mm, respectively. Compared with the original shed-cable support, it is reduced by 931 mm and 794 mm, respectively. The deformation of the surrounding rock is effectively controlled during the excavation and mining, which verifies the effectiveness of the BMC-S. The field control effect is shown in Figure 16.

6. Conclusion

(1) Compared with shed-cable support, BMC-S can effectively improve the stress environment of the surrounding rock in the extremely soft coal seam, increase the range of compressive stress zone, reduce the stress gradient of surrounding rock, and reduce the possibility of tension and shear failure

(2) The displacement difference of the shallow surrounding rock is very small, which effectively inhibits the interlayer dislocation and sliding of the joint in the surrounding rock, reduces the damage to the surrounding rock, and is conducive to maintaining the continuity and stability of the coal

(3) The BMC-S has a good stress state. The coupling and coordination between the high pretightening cable and the high stiffness protective surface components ensure the role of BMC-S in the surrounding rock control of the extremely soft coal roadway

(4) BMC-S forms large and small load-loading arches in the surrounding rock of the roadway in the extremely soft coal seam. The two are superimposed on each other in the surrounding rock to form a large load-loading arch, which significantly inhibits the deformation and failure of the surrounding rock in the arch and the development of joint fissures, and jointly withstands the deformation load of rock mass outside the arch

(5) The engineering practice shows that after the BMC-S technology is adopted, the maximum convergence of the roof and floor is 89 mm, the maximum convergence of two sides is 70 mm, and the mining periods are 192 mm and 187 mm, respectively. Compared with the original shed-cable support, it is reduced by 79% and 76%, respectively. The roadway section meets the requirements of safety production

Data Availability

Conflicts of Interest

The authors declare that they have no conflicts of interest.

Acknowledgments

The work was supported by the National Natural Science Foundation of China (52174138). The authors gratefully acknowledge the financial support of the agency mentioned above.

References

[1] J. X. Tang, Y. L. Wang, G. J. Shu, Z. Y. Dai, and S. Liu, "Study on failure mechanism and control of surrounding rock of mining roadway in high stress ' three soft ' coal seam," *Journal of Mining and Safety Engineering*, vol. 35, no. 3, pp. 449–456, 2018.

[2] B. Q. Meng, J. L. Han, J. Zhang, S. Y. Wen, F. G. Zhang, and H. Li, "Research and application of deep high stress broken soft rock roadway support technology," *Journal of Central South University (Natural Science Edition)*, vol. 47, no. 11, pp. 3861–3872, 2016.

[3] J. Zhang, T. Yang, B. Wang, Q. Xiao, D. Liu, and W. Wang, "Deformation and failure of soft rock roadway and supporting countermeasures in Wangwa coal mine," *Journal of Mining and Safety Engineering*, vol. 32, no. 3, pp. 518–522, 2015.

[4] X. M. Sun, M. C. He, and X. J. Yang, "Study on nonlinear design method of bolt-mesh-cable coupling support in deep soft rock roadway," *Geotechnical Mechanics*, vol. 7, no. 8, pp. 1061–1065, 2006.

[5] K. Nishi, "Creep characteristic of soft rock," *Journal of the Japan Society of Engineering Geology*, vol. 38, no. 5, pp. 304–311, 1997.

[6] L. T. Cheng, J. L. Zhang, Z. S. Zou, and Q. B. Li, "Reasons and control countermeasures of special soft coal roadway deformation in Liangbei coal mine," *Advanced Materials Research*, vol. 671, pp. 1144–1149, 2013.

[7] D. Chen, C. Ji, S. Xie et al., "Deviatoric stress evolution laws and control in surrounding rock of soft coal and soft roof roadway under intense mining conditions," *Advances in Materials Science and Engineering*, vol. 2020, Article ID 5036092, 18 pages, 2020.

[8] M. Karami and A. Tolooiyan, "Investigating the elastoplasticity of an Australian soft rock based on laboratory test results," *Engineering Geology*, vol. 276, article 105762, 2020.

[9] M. C. He, Y. Yuan, X. L. Wang, Z. Q. Wu, C. Liu, and Y. L. Jiang, "Large deformation control technology of Mesozoic composite soft rock in Xinjiang and its application," *Journal of Rock Mechanics and Engineering*, vol. 32, no. 3, pp. 433–441, 2013.

[10] X. F. Wang, Y. Wang, and D. S. Zhang, "Research on strengthening support technology of key parts of roadway in large dip angle ' three soft ' coal seam," *Journal of Mining and Safety Engineering*, vol. 34, no. 2, pp. 208–213, 2017.

[11] S. G. Jing, L. H. Lu, and J. Jiang, "The research and application of the formation mechanism of anchorage structure of roadway in thick coal seam in sliding structure area," *Journal of Mining and Safety Engineering*, vol. 34, no. 5, pp. 928–932, 2017.

[12] S. G. Jing, Q. Z. Wang, and J. Chen, "Deep ' three soft ' coal roadway shed-cable strengthening control mechanism research," *Journal of Mining and Safety Engineering*, vol. 31, no. 3, pp. 938–944, 2014.

[13] Y. Yu, J. B. Bai, X. Wang, W. L. Shen, and C. J. Lian, "Asymmetric deformation and failure characteristics and stability control of soft rock roadways," *Journal of Mining and Safety Engineering*, vol. 31, no. 3, pp. 340–346, 2014.

[14] W. J. Yu, T. Feng, W. J. Wang et al., "Deformation mechanism and control principle and technology of surrounding rock in soft half-coal rock roadway," *Journal of Rock Mechanics and Engineering*, vol. 33, no. 4, pp. 658–671, 2014.

[15] W. J. Yu, W. J. Wang, W. Z. Huang, and H. Wu, "Deformation and failure mechanism and repair control technology of high stress soft rock roadway," *Journal of Coal*, vol. 39, no. 4, pp. 614–623, 2014.

[16] R. L. Dan, Z. T. Yu, X. S. Kong, and Y. Xia, "Soft broken surrounding rock roadway strong angle support control technology," *Coal science and technology*, vol. 41, no. 11, pp. 25–29, 2013.

[17] D. F. Yun, C. Y. Wang, P. Z. Su et al., "Supporting technology of soft roof coal mining roadway with large dip angle," *Coal Science and Technology*, vol. 38, no. 10, pp. 13–16, 2010.

[18] J. T. Lu, J. J. Liu, B. Wang, Z. H. Li, and J. P. Wei, "Surrounding rock activity law and supporting numerical analysis of soft coal roadway in thick coal seam," *Journal of Xi 'an University of Science and Technology*, vol. 30, no. 3, pp. 275–279, 2010.

[19] Q. X. Huang, B. L. Dong, G. H. Chen, L. M. Ran, and Z. P. Huang, "Failure mechanism and bolt - mesh support design of steep - inclined soft coal roadway," *Journal of Mining and Safety Engineering*, vol. 23, no. 3, pp. 333–336, 2006.

[20] X. K. Wang, W. B. Xie, S. G. Jing, Z. L. Su, L. H. Li, and L. H. Lu, "Experimental study on large deformation control mechanism of surrounding rock of extremely loose coal roadway in sliding structural area," *Journal of Rock Mechanics and Engineering*, vol. 37, no. 2, pp. 312–324, 2018.

[21] S. B. Li, L. Wang, C. Q. Zhu, and Q. Ren, "Research on mechanism and control technology of rib spalling in soft coal seam of deep coal mine," *Advances in Materials Science and Engineering*, vol. 2021, Article ID 2833210, 9 pages, 2021.

[22] J. Guo, J. G. Rubino, S. Glubokovskikh, and B. Gurevich, "Effects of fracture intersections on seismic dispersion: theoretical predictions versus numerical simulations," *Geophysical Prospecting*, vol. 65, no. 5, pp. 1264–1276, 2017.

[23] Z. H. Zhao, X. J. Gao, Y. L. Tan, and Q. Ma, "Theoretical and numerical study on reinforcing effect of rock-bolt through composite soft rock-mass," *Journal of Central South University*, vol. 25, no. 10, pp. 2512–2522, 2018.

[24] Z. G. Tao, Q. Geng, C. Zhu et al., "The mechanical mechanisms of large-scale toppling failure for counter-inclined rock slopes," *Journal of Geophysics and Engineering*, vol. 16, no. 3, pp. 541–558, 2019.

[25] E. Mikhail, E. Gabriel, and S. Igor, "Numerical simulation of roof cavings in several Kuzbass mines using finite- difference continuum damage mechanics approach," *International journal of mining science and technology*, vol. 30, no. 2, pp. 157–166, 2020.

[26] W. Zhao, S. C. Wu, Y. T. Gao, Y. Zhou, and S. Xiao, "Numerical simulation of jointed rock mass and determination of mechanical parameters," *Journal of Engineering Science*, vol. 37, no. 12, pp. 1542–1549, 2015.

[27] Y. Wang, H. N. Yang, J. Q. Han, and C. Zhu, "Effect of rock bridge length on fracture and damage modelling in granite containing hole and fissures under cyclic uniaxial increasing-amplitude decreasing-frequency (CUIADF) loads," *International Journal of Fatigue*, vol. 158, article 106741, 2022.

[28] L. I. Hongtao, W. U. Xiangye, H. A. Zhen, Z. H. Xidong, and G. U. Xiaofei, "Evolution law and stability control of plastic zones of retained entry of working face with double roadways layout," *Journal of Mining and Safety Engineering*, vol. 34, no. 4, pp. 689–697, 2017.

[29] F. F. Wu, X. Yue, J. X. Yang, B. du, J. Zhang, and B. Lv, "Model of overlying strata structure in large mining height excavating condition and calculation of support working resistance," *Geofluids*, vol. 2022, Article ID 5894735, 16 pages, 2022.

[30] F. Wu, X. Yu, G. Zhao, B. Du, B. Lv, and J. Zhang, "Characteristics of stress field and damage law of coal rock in residual pillar of top slice and its application," *Frontiers in Earth Science*, vol. 10, p. 122, 2022.

[31] X. L. Zhao and B. X. Huang, "Evaluation of hydraulic fracturing stress disturbance based on stress growth rate and stress gradient," *Journal of Mining and Safety Engineering*, vol. 38, no. 6, pp. 1167–1177, 2021.

[32] Q. Li, J. Hou, T. Han, H. Liu, and S. J. Wang, "Yangzhuang coal mine deep rectangular coal roadway surrounding rock failure characteristics and support technology," *Journal of China University of Mining and Technology*, vol. 45, no. 6, pp. 1124–1131, 2016.

[33] G. B. Li, *Stability Analysis and Control Technology Research of Surrounding Rock of Large Section Roadway in Ganhe Coal Mine*, China University of Mining and Technology (Beijing) Press, 2013.

[34] C. Zhu, M. Karakus, M. He et al., "Volumetric deformation and damage evolution of Tibet interbedded skarn under multistage constant-amplitude-cyclic loading," *International Journal of Rock Mechanics and Mining Sciences*, vol. 152, article 105066, 2022.

[35] W. J. Wang, C. Yuan, W. J. Yu et al., "Control technology of reserved deformation of surrounding rock in deep high stress roadway," *Journal of Coal*, vol. 41, no. 9, pp. 2156–2164, 2016.

[36] F. F. Wu, X. Yu, J. Zhang, Q. Zhou, Z. Gao, and S. Liu, "Research on interaction relationship between support and surrounding rock in fault structural area and its application," *Lithosphere*, vol. 2022, no. Special 11, article 6997956, pp. 1–14, 2022.

[37] R. Pan, Y. Cai, H. X. Huang et al., "Study on abutment pressure distribution and stress law of support components in three soft coal seams," *Journal of Mining and Safety Engineering*, vol. 38, no. 6, pp. 1091–1099, 2021.

[38] Y. L. Xu, M. T. Xu, and L. X. Cheng, "Control principle and experimental study on load-loading arch of roadway reconstruction under strong dynamic pressure," *Journal of Mining and Safety Engineering*, vol. 35, no. 6, pp. 1135–1141, 2018.